Parameter-free model to estimate thermal conductivity in nanostructured materials

Giuseppe Romano, Alexie M. Kolpak, Jesús Carrete, and David Broido

A Parameter-Free Model to Estimate the Thermal Conductivity in Nanostructured Materials

Giuseppe Romano* and Alexie M. Kolpak
Department of Mechanical Engineering, Massachusetts Institute of Technology,
77 Massachusetts Avenue, Cambridge, MA 02139, USA

Jesús Carrete
Institute of Materials Chemistry, TU Wien, A-1060 Vienna, Austria

David Broido
Department of Physics, Boston College, Chestnut Hill, Massachusetts 02467, USA

Achieving low thermal conductivity and good electrical properties is a crucial condition for thermal energy harvesting materials. Nanostructuring offers a very powerful tool to address both requirements: in nanostructured materials, boundaries preferentially scatter phonons compared to electrons. The computational screening for low-thermal-conductivity nanostructures is typically limited to materials with simple crystal structures, such as silicon, because of the complexity arising from modeling branch- and wave vector-dependent nanoscale heat transport. The phonon mean-free-path (MFP) dependent Boltzmann transport equation (MFP-BTE) approach is a model that overcomes this limitation. To illustrate this, we analyze thermal transport in 75 nanoporous half-Heusler compounds for different pore sizes. Our calculations demonstrate that, in most cases, the optimization of thermal transport in nanostructures should take into account both bulk thermal properties and geometry-dependent size effects, two aspects that are typically engineered separately. To enable efficient calculations within this paradigm we derive a model, based on the "gray" formulation of the BTE, that can decouple the influence of the geometry and the material on the effective thermal conductivity with relatively little loss in accuracy compared to the MFP-BTE. Our study motivates the need for a holistic approach to engineering thermal transport and provides a method for high-throughput low-thermal conductivity materials discovery.

INTRODUCTION

Direct conversion of thermal energy into electricity has tremendous advantages in many applications, including power generation and cooling [1, 2]. Despite decades of research on thermoelectric materials, the energy conversion efficiency is still relatively low compared to traditional technologies. The thermoelectric efficiency in semiconductors is limited by the figure of merit $ZT = T\sigma S^2/\kappa$, where σ is the electrical conductivity, S is the Seebeck coefficient, T the lattice temperature and κ is the thermal conductivity (TC), which consists of electronic and lattice components: κ_{el} and κ_L. As these three quantities are interrelated, achieving high-ZT materials is challenging. Nanostructuring is a unique platform to overcome some of these challenges because it preferentially suppresses phonon transport relative to electrical transport [3]. The reason for such behaviour stems from the fact that phonon mean free paths (MFPs) are typically larger than electron MFPs that contribute to σ in heavily-doped semiconductors. Promising results have been obtained with nanowires [4–7], thin films [8, 9] and porous materials [10–16]. As phonons may have wide MFP distributions, effective suppression can be achieved with all-scale hierarchical materials. The different scales can be spanned by combining doping, nano-inclusion and grain engineering [17].

For practical reasons, the search for low TC bulk materials is often pursued separately from the engineering of phonon suppressing nanostructures. A common simplification is that given two materials with bulk TCs κ_a and κ_b with $\kappa_b > \kappa_a$, this ordering is preserved in their nanostructured counterparts. In this work, we challenge this assumption by calculating the TC of porous materials based on half-Heusler (HH) compounds; the bulk MFP distributions are taken from [18]. Our model, based on the phonon Boltzmann transport equation (BTE) and first-principles calculations, predicts that the bulk ordering is largely preserved only for structures with nanostructuring length scales that are relatively large with respect to the bulk MFP distribution. Conversely, when heat is primarily ballistic, the bulk MFP distribution plays a crucial role in determining the ordering of the TCs. The nanostructuring length scale, referred to as "characteristic length" throughout the text, is the limiting dimension of the material, e.g. the thickness of a thin film. Finally, we identify a material-independent model, based on a simplified version of the BTE, that provides a faster estimation of the TC of a given nanostructure and a generic set of materials. As HHs are promising thermoelectric materials [19–21], our work provides practical guidance to experimentalists. Furthermore, it can serve as a basis for high-throughput thermal transport in nanostructures, where the bulk MFP distribution can be estimated from either first-principles or experimental

reconstructions of MFP distributions [22, 23]. Finally, it demonstrates that effective material optimization should explicitly include both intrinsic materials properties and system geometries.

RESULTS

The crystal structure of the HH compound ABC is formed by three interpenetrating FCC lattices, where A and C form a rocksalt structure and B is located at the diagonal position $(1/4, 1/4, 1/4)$, as shown in Fig. 1(a). The 75 HH compounds considered in this work are taken from Ref. [18], in which high-throughput calculations were used to screen nearly 80 thousand entries from the AFLOW database [24], on the basis of mechanical and thermodynamic stability. Similarly to Ref. [25], we consider a nanoporous material with circular pores arranged on a square lattice. The simulation domain is a unit cell that comprises a single pore and has periodicities $L = 10$ nm, 100 nm, or 1 μm. We note that, in this case, the periodicity is equal to distance between the centers of the pores, i.e. the pitch. The thickness of the material is considered to be infinite. The porosity, *i.e.*, the ratio of the pore volume to the total volume, is fixed to $\phi = 0.3$; the pores diameter is ≈ 6.18 nm, 61.8 nm and 618 nm for L $= 10$ nm, 100 nm and 1μm, respectively. Periodic boundary conditions are applied to the heat flux on the boundaries of the unit cell. Along the walls of the pore we apply diffuse scattering boundary conditions, *i.e.*, incoming phonons are scattered back isotropically; the temperature of the phonons leaving the pore's surface is set so that zero normal thermal flux is guaranteed along the boundary [26]. Heat flux is ensured by applying a temperature difference $\Delta T = 1$ K between the hot and cold contacts. A sketch of the simulation domain is shown in Fig. 1(a). Our model for phonon transport is based on the MFP-BTE [27, 28]

$$\Lambda \hat{\mathbf{s}} \cdot \nabla T(\mathbf{r}, \Lambda) + T(\mathbf{r}, \Lambda) = T_L(\mathbf{r}), \qquad (1)$$

where $T(\mathbf{r})$ is the space-dependent effective temperature distribution of phonons with MFP Λ and group velocity with direction $\hat{\mathbf{s}}$; $T_L(\mathbf{r})$ is the effective lattice temperature, given by

$$T_L(\mathbf{r}) = \int_0^\infty < T(\mathbf{r}, \Lambda') > B_2(\Lambda')d\Lambda', \qquad (2)$$

where $< . >$ is an angular average and $B_n(\Lambda') = \left[\int_0^\infty K(\Lambda'')/\Lambda''^n d\Lambda''\right]^{-1} K(\Lambda')/\Lambda'^n$. The term $K(\Lambda)$ is the bulk MFP distribution, computed by combining density functional theory (DFT) with the phonon supercell approach [29, 30]. The implementation of our BTE model is described elsewhere [27, 28]. For clarity, we will drop all the space dependencies from the notation. Along

the walls of the pore we apply diffuse scattering boundary conditions, *i.e.*, incoming phonons are scattered back isotropically; the temperature of the phonons leaving the pore's surface, T_B, is set so that zero normal thermal flux is guaranteed along the boundary and is given by [26]

$$T_B = \int B_1(\Lambda)T_+(\Lambda)d\Lambda, \qquad (3)$$

where $T_+(\Lambda) = 1/4 < T(\Lambda)\hat{\mathbf{s}} \cdot \hat{\mathbf{n}} >_+ \cdot \hat{\mathbf{n}}$; the notation $< f >_+$ stands for an angular average over all incoming phonons and $\hat{\mathbf{n}}$ is the normal to the boundary. The essence of classical size effects is captured by the phonon suppression function

$$S(\Lambda) = \frac{3L}{\Delta T A_{\text{Hot}}\Lambda} \int_{A_{\text{Hot}}} < T(\Lambda)\hat{\mathbf{s}} > \cdot \hat{\mathbf{n}}dS, \qquad (4)$$

a quantity that describes the ratio of the MFP distribution of the porous material to that of the bulk $K(\Lambda)$, where Λ is the bulk MFP. In Eq. 4, A_{hot} is the surface area of the hot contact. Once $S(\Lambda)$ is computed by the BTE, the effective TC is obtained via

$$\kappa_{eff} = \int_0^\infty K(\Lambda)S(\Lambda)d\Lambda =$$
$$= \int_0^\infty \alpha_{\text{bulk}}(\Lambda)g(\Lambda)d\Lambda, \qquad (5)$$

where $g(\Lambda) = -\partial S(\Lambda)/\partial \Lambda$ and $\alpha_{\text{bulk}}(\Lambda)$ is the cumulative bulk thermal conductivity at MFP Λ, *i.e.* the sum of all MFP contributions up to Λ. We note the bulk TC is $\kappa_{\text{bulk}} = \int_0^\infty K(\Lambda)d\Lambda$. The values for κ_{bulk} at room temperature of the HH compounds considered in this study range from 1.24 WK^{-1}m^{-1} (NiHfSn) to 62.12 WK^{-1}m^{-1} (CoNbSn) [18]. When the porous material is large enough that all phonons travel diffusively, κ_{eff} is obtained by Fourier's law, i.e.

$$\kappa_{\text{Fourier}} = -\kappa_{\text{bulk}}\frac{L}{\Delta T A_{\text{hot}}} \int_{A_{\text{hot}}} \nabla T_F \cdot \hat{\mathbf{n}}dS, \qquad (6)$$

where the temperature T_F is the solution to $\nabla^2 T_F = 0$. In the case of aligned pores, the reduction factor, $\kappa_{\text{Fourier}}/\kappa_{\text{bulk}} \approx r = (1-\phi)/(1+\phi) = 0.54$, is predicted by Eucken-Garnett theory [31] and is in agreement with that computed by our Finite-Volume (FV) diffusive solver. As diffusive heat conduction does not depend on the phonon MFPs, it gives the same result regardless the size of the unit cell, as long as the porosity is kept constant. Conversely, when size effects occur, heat transport becomes scale dependent [32, 33] and degrades significantly. In fact, our BTE simulations predict that the values of κ_{eff} are on average 17 %, 65 % and 83 % smaller than those computed by Fourier's law. These reductions are in line with those obtained by Monte Carlo simulations on similar structures [33]. In the subsequent analysis, to focus on size effects we normalized κ_{eff} by the macroscopic reduction factor, i.e. $\tilde{\kappa} = \kappa_{\text{eff}}\kappa_{\text{bulk}}/\kappa_{\text{Fourier}} = \kappa_{\text{eff}}r^{-1}$. In

Fig. 2(a), we plot the distribution of $\tilde{\kappa}$ for all compounds and periodicities. We note that for L = 10 nm, most of the values are below 10 Wm^{-1}K^{-1}, as a result of suppression of long-MFP phonons. As L increases, the distribution of $\tilde{\kappa}$ widens up until approaching the bulk one for L = 1 μm, where size effects become negligible. The values of $\tilde{\kappa}$ are available upon request.
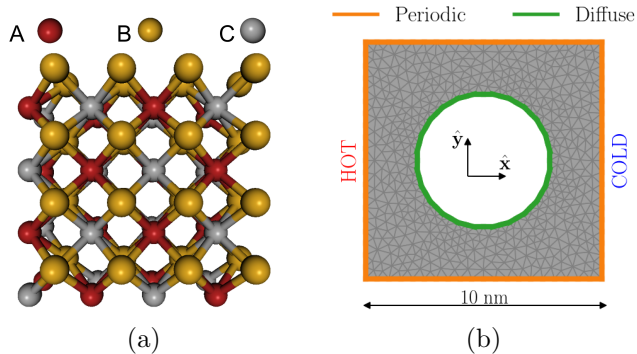

FIG. 1. (a) Structure of the HH compound. ABC are three generic elements sitting on three interpenetrating fcc lattices. (b) Unit cell used for the BTE calculation. Heat flux is set up by imposing a difference of temperature between the hot and cold contacts.

We now assess whether κ_{bulk} can be used as a "descriptor" for $\tilde{\kappa}$. A descriptor is a simple model correlated, within some approximation, to a more complicated calculation. The linear regression between κ_{bulk} and $\tilde{\kappa}$ is shown in Fig. 2(b). We quantify their correlation with the Spearman rank correlation [34]; such a quantity correlates the ranking of two variables within their corresponding sets. If the ranking is fully preserved, $r_s = 1$. In our case we obtain $r_s \approx 0.88, 0.96, 1$ for L = 10 nm, 100 nm and 1 μm, respectively. This trend can be understood if we analyze the phonon suppression functions. To this end, we conveniently introduce the Knudsen number, Kn, as the ration between the MFP and the limiting dimension of a material, e.g. the pore-pore distance in a porous materials. For small Kns, phonons travel mostly diffusively and $S(\Lambda)$ reaches a plateau; consequently, when L_c is larger than the MFPs of heat-carrying phonons, e.g. for L = 1 μm, the shape of $S(\Lambda)$ in the non-diffusive regime becomes negligible with $\tilde{\kappa}$ being determined completely by κ_{bulk}. However, for smaller periodicities the entire curve $S(\Lambda)$ must be taken into account. In fact, as shown in Fig. 3(a), for L = 10 nm $S(\Lambda)$ strongly depends on the material while for L = 100 nm the suppression functions approaches a universal value, called diffusive material limit [26]. Such a limit assumes that all phonon MFPs are smaller than L_c and is practically achieved with L= 1 μm. On the other extreme, when all the MFPs are larger than L_c, we have the ballistic material limit, also plotted in Figs. 3(a) and 3(b). To enable fast calculations of size effects in complex geometries

and with a wide library of bulk materials, we set out to derive a material- and scale- independent approximation to $S(\Lambda)$. In a first attempt, we build a model assuming that heat carried by phonons with MFP smaller than a generic threshold Λ_T does not suffer size effects, while all the rest is completely suppressed. The term Λ_T is a parameter that we vary within a range that is chosen to be larger than the bulk MFPs; each choice of Λ_T leads to a different value of the effective thermal conductivity. Within this approximation, the suppression function is given by $S(\Lambda) = r\Theta(\Lambda_T - \Lambda)$, where $\Theta(x)$ is the Heaviside function. Using Eq. 5, we get $g(\Lambda) = r\delta(\Lambda - \Lambda_T)$ and $\tilde{\kappa} \approx \kappa_\delta = \alpha_{\text{bulk}}(\Lambda_T)$. This result shows that $\tilde{\kappa}$ is dictated by the bulk cumulative thermal conductivity around Λ_T rather than by κ_{bulk}. In fact, there are cases, such as for the pair CoBiTi and RuTaSb, where the curves of α_{bulk} cross each other for some values of Λ_T (see Fig. 2(c).) In this instance, if the nanostructuring length is smaller than the crossing point the ordering of κ_{bulk} is the opposite to that of $\tilde{\kappa}$, an effect that is captured by $\tilde{\kappa}_\delta$. For completeness, we note that there are cases, such as the pair CoNbSi-RhBiTi (see inset of Fig. 2(c)), where the ordering swaping is absent. Within the considered library, the number of material pairs with crossing cumulative thermal conductivities is roughly 80 % of the total number of pairs, further motivating the need for a model that goes beyond Fourier's heat conduction. In carrying this analiysis we have ruled out pairs of materials where whe crossing point is below 3 nm due to the challenges in fabricating nanostructures with smaller geometric features. It is worth noting that the effect of ordering mismatch has already been discussed conceptually in [35].

In this section we assess the use of κ_δ as a descriptor for $\tilde{\kappa}$. To this end we calculate the Spearman rank correlation between these two quantities for different Λ_T. As shown in Fig. 2(d), for all the periodicities such a correlation increases with Λ_T, reaches a maximum, and eventually approaches a constant value. These final values concide with those obtained with κ_{bulk} as a decriptor since $\alpha_{\text{bulk}}(\infty) = \kappa_{\text{bulk}}$, namely there is no size effects. The value at which the correlation is maximum increases with L, as a consequence of the increasing characteristic length, referred to as L_c. These results show, therefore, that by taking into account α_{bulk} the ordering of $\tilde{\kappa}$ within a given set of materials is better estimated than with the simple use of κ_{bulk}. However, this descriptor has a limitation: the optimal Λ_T for a given structure is unknown unless one runs the BTE, negating the utility of κ_δ. We note that, in principle, one can estimate Λ_T on the basis of the characteristic lenght of the material; however, such a property is cumbersome to identify in complex geometries. Motivated by this shortcoming, we introduce a parameter-free descriptor, as detailed below.

The material dependency arises from the definition of T_L in Eq. 2, encoding the fact that the material is *nongray*. The hypothesis of gray materials, on the other
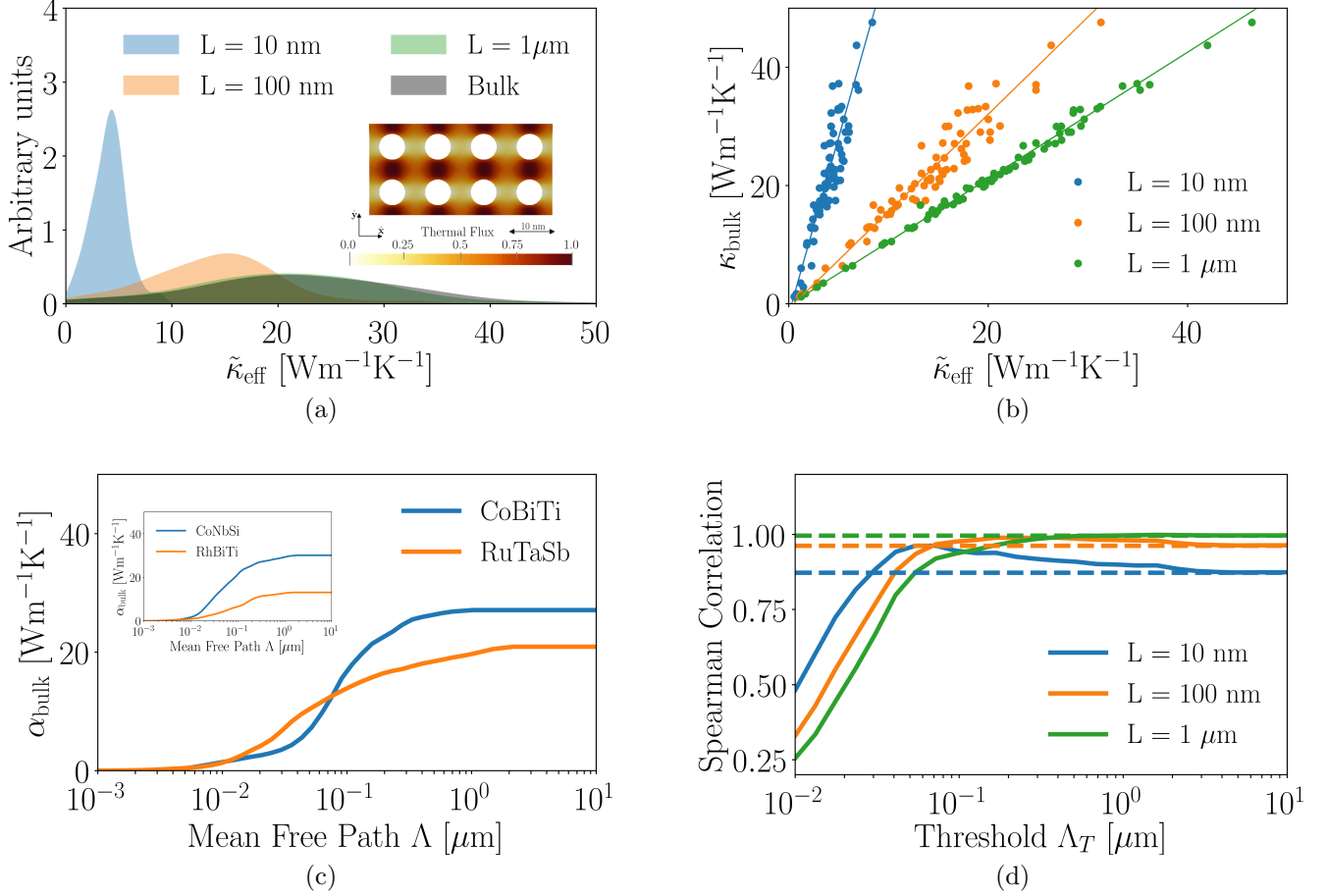
FIG. 2. (a) Thermal conductivity ($\tilde{\kappa}$) density distributions for L = 10 nm, 100 nm and 1 μm. As the periodicity increases the values of $\tilde{\kappa}$ approach those of the bulk because size effects become negligible. The inset shows the thermal flux map. The gradient of temperature is enforced along the $\hat{\mathbf{x}}$ direction. Red areas indicate high-flux regions. (b) Linear regression between $\tilde{\kappa}$ and κ_{bulk} for all the periodicities. (c) A representative pair of crossing bulk cumulative thermal conductivities, κ_{bulk}. In the inset, a pair of non-crossing α_{bulk} is illustrated. (d) The Spearman rank correlation between $\kappa_\delta(\Lambda_T)$ and $\tilde{\kappa}$ is shown for all L and varying Λ_T.

hand, assumes that there is only one phonon MFP. Here we adopt a middle-ground approach by solving the BTE for different MFPs, independently. For this reason, we call this model the "multi-gray" (MG) model. We note that this approach is formally equivalent to Ref. [36] but applied to arbitrary geometries. Within this assumption, the BTE becomes

$$\Lambda \hat{\mathbf{s}} \cdot \nabla T(\Lambda) + T(\Lambda) = <T(\Lambda)>. \quad (7)$$

We note that as $\int B_2(\Lambda)d\Lambda = 1$, T_L is always bounded by the extreme values of $<T(\Lambda)>$. As a consequence, by choosing $<T(\Lambda)>$ as a material-independent effective lattice temperature, we make it sure that the error with respect to T_L does not increase unreasonably. Furthermore, it is possible to show that this model conserves the energy for each choice of Λ [27, 32, 37].

After Eq. 7 is solved for a wide range of MFPs, we compute the phonon suppression function, $S_{\text{MG}}(\Lambda)$, us-

ing Eq. 4. We point out that Eq. 4 does not make any assumption on T_L thus it holds for both the MFP-BTE and MG models. Then, we evaluate $\tilde{\kappa}_{\text{MG}} = r^{-1} \int_0^\infty S_{\text{MG}}(\Lambda)K(\Lambda)d\Lambda$. The Spearmen rank correlation between $\tilde{\kappa}_{\text{MG}}$ and $\tilde{\kappa}$ is close to unity for all the periodicities, and the linear regression slopes are 0.89, 0.94 and 0.97, for L = 10 nm, 100 nm and 1 μm, respectively (Fig. 3(c).) This trend can be understood if we analyze phonon suppression in the small-Kn limit, namely where the difference between $S_{\text{MG}}(\Lambda)$ and $S(\Lambda)$ reaches, generally, its maximum value. In the MG case, it is possible to show that $S_{\text{MG}}(0) = r$, i.e. it recovers the standard diffusive limit. On the other hand, combining Eqs. 1-2-4, the suppression function, computed at $\Lambda = 0$, gives

$$S(0) = -\frac{3L}{A_{\text{hot}}} \int_{A_{\text{hot}}} B_2(\Lambda)\nabla <T(\Lambda)> \cdot \hat{\mathbf{n}}dSd\Lambda; \quad (8)$$
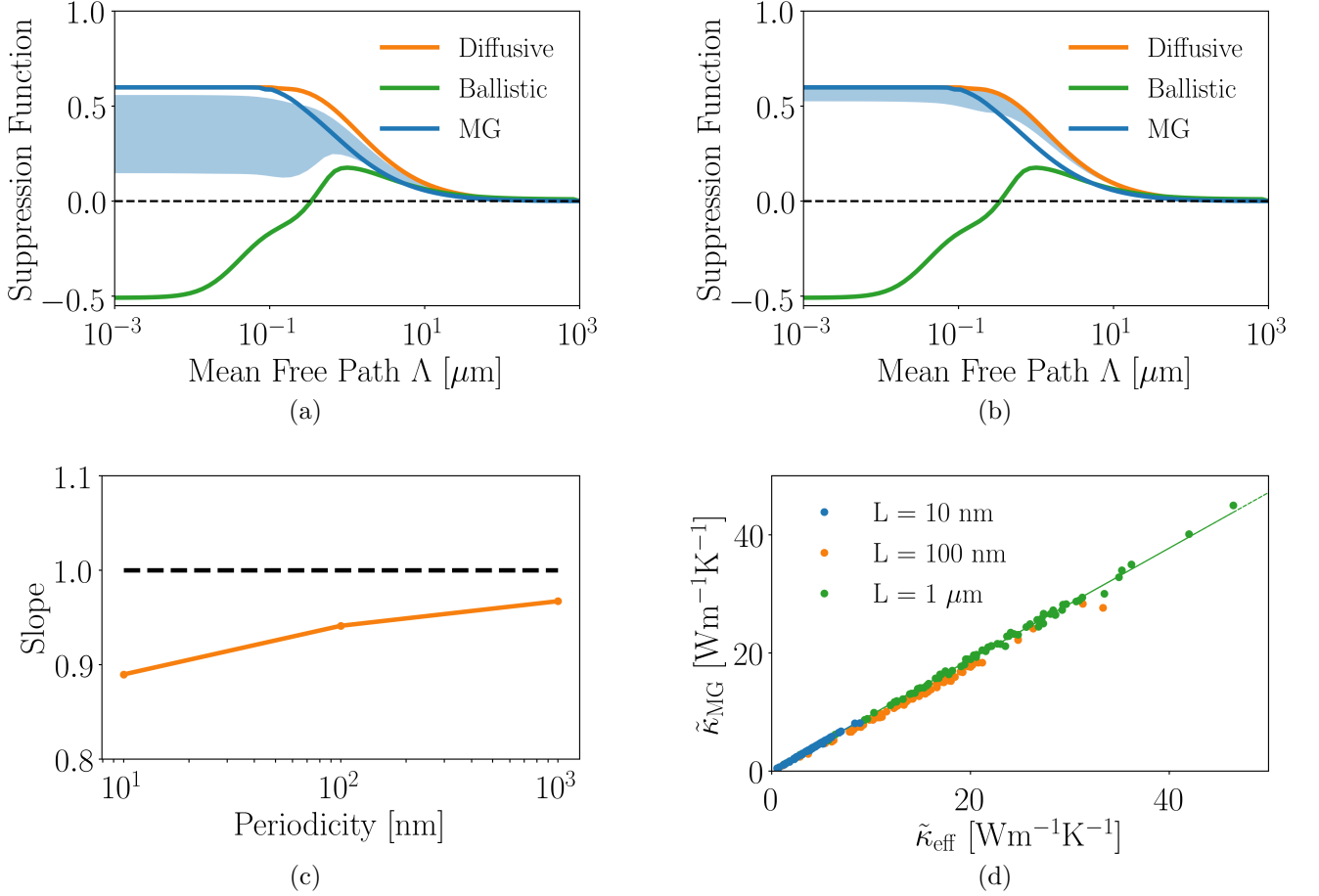
according to [26], the gradient of $<T(\Lambda)>$ reaches a

FIG. 3. Suppression functions of the HH compounds (blue shaded region) for (a) L = 10 nm and (b) L = 100 nm. These curves are bounded by those of the "diffusive" and "ballistic" material limits. The suppression function of the "multiple gray" model is also plotted. (c) The slope of the regression model between $\kappa_{\rm eff}$ and $\tilde{\kappa}_{\rm MG}$. The value 1 represents perfect quantitative prediction. (d) The regression model between $\tilde{\kappa}$ and $\tilde{\kappa}_{\rm MG}$.

plateau for small Kns. Therefore, for macroscopic materials, i.e. when all the phonon MFPs are smaller than the characteristic length, Eq. 9 becomes

$$S(0) \approx -\frac{3L}{A_{\rm hot}} \int_{A_{\rm hot}} \nabla < T(0) > \cdot \hat{\mathbf{n}} dS \int B_2(\Lambda) d\Lambda. \quad (9)$$

As mentioned above, this is the case of a diffusive material. It is possible to show that, in this regime, $S(0)$ only includes geometric effects thus it is equal to r [26]. For this reason, the performance of $S_{\rm MG}(\Lambda)$ in estimating $S(\Lambda)$ increases with the size of the unit cell. However, when considering materials with strong size effects, the two quantities may differ; this difference may be estimate by looking at the fraction of MFPs falling below the characteristic length.

The definition of the MG model allows us to calculate a suppression function that does not depend on the bulk material. In fact the bulk MFP distribution is taken into account only in Eq. 5, which has a negligible cost. Therefore, once the MG model is evaluated for a given

geometry, the calculations of $\tilde{\kappa}$ for a set of new bulk materials come, practically, with no additional computational effort. Moreover, if we define a geometry only in terms of relative distances, we may also compute $\tilde{\kappa}$ for different scales with no added cost. In fact, scaling Eq. 7 by a space variable, which we choose to be L, we have

$$\xi \,\hat{\mathbf{s}} \cdot \nabla T(\xi) + T(\xi) = < T(\xi) >, \quad (10)$$

where $\xi = \Lambda L^{-1}$. The suppression function for the MG model thus becomes a function of the relative dimension ξ. Hence, once $S_{MG}(\xi)$ is computed, $\tilde{\kappa}$ can be evaluated for arbitrary scales via

$$\tilde{\kappa}_{MG}(L) = r^{-1} \int K(\xi L) S_{\rm MG}(\xi) d\xi. \quad (11)$$

Ideally, $S_{\rm MG}(\xi)$ must be evaluated for $\xi \in \mathbb{R}$. However, on the basis that ξ is nothing than the Knudsden number with the characteristic length set to L, $S_{\rm MG}(\xi)$ can be approximated to r for small ξ. On the other hand, for

large ξ, we may use $S_{\mathrm{MG}}(\xi) \approx \alpha\xi^{-1}$, where α can be retrieved by fitting such trend as we approach the ballistic regime.

CONCLUSION

By solving the phonon Boltzmann transport equation, we have computed the effective thermal conductivity of 75 nanoporous half-Heusler compounds with different periodicities, obtaining significant reductions with respect to the corresponding bulk values. Then, we have developed a model that enables the calculation of thermal transport in a large number of materials by solving the BTE only once, within a given geometry. In addition to enhancing our understanding of nanoscale heat transport, our approach has the potential of accellerating materials discovery for thermoelectric applications.

ACKNOWLEDGEMENTS

———————

* romanog@mit.edu

[1] D. M. Rowe, ed., *CRC Handbook of Thermoelectrics* (CRC Press, Boca Raton, FL, 1995).

[2] G. J. Snyder and E. S. Toberer, in *Materials For Sustainable Energy: A Collection of Peer-Reviewed Research and Review Articles from Nature Publishing Group* (World Scientific, 2011) pp. 101–110.

[3] C. Vineis, A. Shakouri, A. Majumdar, and M. Kanatzidis, Adv. Mater. **22**, 3970 (2010).

[4] A. I. Hochbaum, R. Chen, R. D. Delgado, W. Liang, E. C. Garnett, M. Najarian, A. Majumdar, and P. Yang, Nature **451**, 163 (2008).

[5] A. I. Boukai, Y. Bunimovich, J. Tahir-Kheli, J.-K. Yu, W. A. Goddard III, and J. R. Heath, Nature **451**, 168 (2008).

[6] Y.-M. Lin, X. Sun, and M. Dresselhaus, Physical Review B **62**, 4610 (2000).

[7] N. Mingo, Applied Physics Letters **85**, 5986 (2004).

[8] R. Venkatasubramanian, E. Siivola, T. Colpitts, and B. O'Quinn, Nature **413**, 597 (2001).

[9] G. Min, D. Rowe, and F. Volklein, Electronics letters **34**, 222 (1998).

[10] A. M. Marconnet, T. Kodama, M. Asheghi, and K. E. Goodson, Nanosc. Microsc. Therm. **16**, 199 (2012).

[11] J. Lee, J. Lim, and P. Yang, Nano Lett. **15**, 3273 (2015).

[12] J. Tang, H.-T. Wang, D. H. Lee, M. Fardy, Z. Huo, T. P. Russell, and P. Yang, Nano Lett. **10**, 4279 (2010).

[13] D. Song and G. Chen, Appl. Phys. Lett. **84**, 687 (2004).

[14] P. E. Hopkins, C. M. Reinke, M. F. Su, R. H. Olsson, E. A. Shaner, Z. C. Leseman, J. R. Serrano, L. M. Phinney, and I. El-Kady, Nano Lett. **11**, 107 (2011).

[15] M. R. Wagner, B. Graczykowski, J. S. Reparaz, A. El Sachat, M. Sledzinska, F. Alzina, and C. M. Sotomayor Torres, Nano letters **16**, 5661 (2016).

[16] S. Gluchko, R. Anufriev, R. Yanagisawa, S. Volz, and M. Nomura, Applied Physics Letters **114**, 023102 (2019).

[17] K. Biswas, J. He, I. D. Blum, C.-I. Wu, T. P. Hogan, D. N. Seidman, V. P. Dravid, and M. G. Kanatzidis, Nature **489**, 414 (2012).

[18] J. Carrete, W. Li, N. Mingo, S. Wang, and S. Curtarolo, Phys. Rev. X **4**, 011019 (2014).

[19] X. Yan, G. Joshi, W. Liu, Y. Lan, H. Wang, S. Lee, J. Simonson, S. Poon, T. Tritt, G. Chen, *et al.*, Nano Lett. **11**, 556 (2010).

[20] S. Sakurada and N. Shutoh, Appl. Phys. Lett. **86**, 082105 (2005).

[21] H. Zhu, R. He, J. Mao, Q. Zhu, C. Li, J. Sun, W. Ren, Y. Wang, Z. Liu, Z. Tang, *et al.*, Nature communications **9**, 2497 (2018).

[22] A. J. Minnich, J. Johnson, A. Schmidt, K. Esfarjani, M. Dresselhaus, K. A. Nelson, and G. Chen, Phys. Rev. Lett. **107**, 095901 (2011).

[23] K. T. Regner, D. P. Sellan, Z. Su, C. H. Amon, A. J. McGaughey, and J. A. Malen, Nat. Commun. **4**, 1640 (2013).

[24] S. Curtarolo, W. Setyawan, G. L. Hart, M. Jahnatek, R. V. Chepulskii, R. H. Taylor, S. Wang, J. Xue, K. Yang, O. Levy, *et al.*, Comput. Mater. Sci. **58**, 218 (2012).

[25] G. Romano, A. Di Carlo, and J. C. Grossman, J. Comput. Electron. **11**, 8 (2012).

[26] G. Romano and A. M. Kolpak, J. Heat Transfer **141**, 012401 (2019).

[27] G. Romano and A. Di Carlo, IEEE Trans. Nanotechnol. **10**, 1285 (2011).

[28] G. Romano and J. C. Grossman, J. Heat Transf. **137**, 071302 (2015).

[29] W. Li, J. Carrete, N. A. Katcho, and N. Mingo, Comput. Phys. Commun. **185**, 1747 (2014).

[30] D. Broido, M. Malorny, G. Birner, N. Mingo, and D. Stewart, Appl. Phys. Lett. **91**, 231922 (2007).

[31] C. Nan, R. Birringer, D. R. Clarke, and H. Gleiter, J. Appl. Phys. **81**, 6692 (1997).

[32] G. Romano, A. Di Carlo, and J. C. Grossman, J. Comput. Electron. **11**, 8 (2012).

[33] D. Chakraborty, S. Foster, and N. Neophytou, Physical Review B **98**, 115435 (2018).

[34] J. Carrete, W. Li, N. Mingo, S. Wang, and S. Curtarolo, Phys. Rev. X **4**, 011019 (2014).

[35] G. Romano, K. Esfarjani, D. A. Strubbe, D. Broido, and A. M. Kolpak, Phys. Rev. B **93**, 035408 (2016).

[36] F. Yang and C. Dames, Phys. Rev. B **87**, 035437 (2013).

[37] J. Y. Murthy, S. V. Narumanchi, P.-G. Jose'A, T. Wang, C. Ni, and S. R. Mathur, International Journal for Multiscale Computational Engineering **3** (2005).